PAPER

Check for updates

High efficiency of nitric acid controls in alleviating particulate nitrate in livestock and urban areas in South Korea†

Haeri Kim, [ID] [a] Junsu Park, [a] Seunggi Kim, [ID] [a] Komal Narayan Pawar [ID] [a] and Mijung Song [ID] *[ab]

Remarkably, enhanced particulate nitrate (NO_3^-) concentrations occur in many environments during particulate matter (PM) pollution; however, information on the formation mechanism and alleviation strategies is still limited. Herein, to explore the NO_3^- formation mechanism and conditions, we measured the concentrations of water-soluble inorganic ions in $PM_{1.0}$ as well as the inorganic gas concentrations of HNO_3, NO_2, and NH_3 in Gimje, a highly dense livestock area, from June to July 2020 and January to February 2021. At the monitoring site, extremely high atmospheric NH_3 was measured with an hourly average of 96.9 ± 48.1 ppb, and the daily average of HNO_3 and $PM_{1.0}$ was 0.7 ± 0.7 ppb, and 20.1 ± 8.8 μg m^{-3}, respectively. A clear increase in the NO_3^- concentration in $PM_{1.0}$ was observed on high pollution days ($PM_{1.0} \geq 20$ μg m^{-3}), suggesting that HNO_3 and NH_3 contributed to NO_3^- formation. Moreover, we applied the thermodynamic model ISORROPIA-II to predict the NO_3^- response to the reduction of total HNO_3 (TN), total NH_3 (TA), and SO_4^{2-}. The results showed that controlling TN could be more effective in alleviating particulate NO_3^- than controlling SO_4^{2-} and TA in the livestock area. We also compared this result to that of a nearby urban area, Jeonju. A similar result was observed, with efficient HNO_3 control, which reduced the NO_3^- concentration in Jeonju. These measurements and simulations indicated that NO_x control could be the most effective approach to reduce particulate NO_3^- concentrations in both livestock and urban areas. Our results provide a significant contribution to developing a strategy for alleviating particulate NO_3^- pollution.

Environmental significance

The particulate nitrate (NO_3^-) concentration is often enhanced during particulate matter (PM) pollution; however, there is limited information on the formation mechanism and reduction strategies of particulate NO_3^-. Using thermodynamic model ISORROPIA-II and the measurements of inorganic gaseous species and water-soluble ions of $PM_{1.0}$, we show that controlling total nitrate could be more effective in reducing particulate NO_3^- and PM concentrations than controlling SO_4^{2-} and total ammonia in a livestock area. Moreover, a similar result was observed with efficient HNO_3 control, which reduced NO_3^- and PM concentrations in a nearby urban area. This suggests that NO_x control is an effective approach to reduce particulate NO_3^- in both livestock and urban areas. In the future, a strategy can be developed to reduce NO_3^- pollution by using the results of this study.

Introduction

Particulate matter (PM) below 2.5 μm in aerodynamic diameter ($PM_{2.5}$) significantly impacts the air quality, global climate, and human health.[1–3] $PM_{2.5}$ is emitted directly into the atmosphere. $PM_{2.5}$ mainly contains ammonium sulfate (($NH_4)_2SO_4$), ammonium nitrate (NH_4NO_3), and organic aerosols formed *via* photochemical reactions of precursor gaseous species such as nitrogen oxides (NO_x), ammonia (NH_3), sulfur dioxide (SO_2), and volatile organic compounds.[4] In $PM_{2.5}$, secondary inorganic aerosols (SIAs) account for more than 80% by mass, depending on the location and season.[5,6]

Among SIAs, the concentration of NH_4NO_3 remarkably increases during $PM_{2.5}$ pollution in various environments.[7–9] NH_4NO_3 can be produced by a series of chemical reactions of NO_x and NH_3, as follows:[4]

$$NO_2 (g) + OH (g) \rightarrow HNO_3 (g) \tag{R1}$$

$$NH_3 (g) + HNO_3 (g) \rightarrow NH_4NO_3 (s, aq) \tag{R2}$$

In the atmosphere, nitrogen dioxide (NO_2) reacts with hydroxyl radicals (OH) to produce nitric acid (HNO_3). HNO_3

[a]Department of Environment and Energy, Jeonbuk National University, Jeonju 54896, Korea
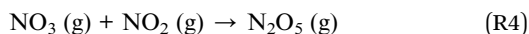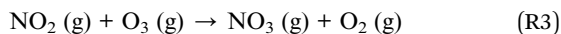
[b]Department of Earth and Environmental Sciences, Jeonbuk National University, Jeonju 54896, Korea

† Electronic supplementary information (ESI) available. See DOI: https://doi.org/10.1039/d2ea00051b

then reacts with NH_3 to form NH_4NO_3. NH_4NO_3 is a semi-volatile species that can partition primarily from the gas-phase to the particle-phase, depending on the temperature.[4]

Studies on night-time chemistry have addressed nitrate (NO_3^-) formation by heterogeneous reactions.[10] During night-time, nitrogen trioxide (NO_3) is produced by the reaction of NO_2 and ozone (O_3) (R3), and the NO_3 reacts with NO_2 to form dinitrogen pentoxide (N_2O_5) (R4). Heterogeneous uptake of N_2O_5 on aerosol surfaces produces HNO_3 *via* hydrolysis (R5).[4]

$$NO_2 \text{ (g)} + O_3 \text{ (g)} \rightarrow NO_3 \text{ (g)} + O_2 \text{ (g)} \quad \text{(R3)}$$

$$NO_3 \text{ (g)} + NO_2 \text{ (g)} \rightarrow N_2O_5 \text{ (g)} \quad \text{(R4)}$$

$$N_2O_5 \text{ (g)} + H_2O \text{ (l)} \rightarrow 2HNO_3 \text{ (aq)} \quad \text{(R5)}$$

These reactions produce particulate NO_3^- under NH_3-rich conditions.[4] However, under NH_3-poor conditions, HNO_3 can be formed through the reaction of other alkaline species.[11]

NO_x and NH_3, the main precursor gases of NH_4NO_3, are emitted into the atmosphere by various sources. NO_x is emitted not only by anthropogenic activities such as combustion of oil and coal, energy generation, on-road transportation, and agricultural activities, but also by natural sources such as soil, biomass burning, and lightning.[12,13] In California[14] and the North China Plain,[15] where there are active agricultural areas, the total NO_x emissions accounted for more than 30% in 2013 and 50% in 2017. NH_3 is mainly emitted from agricultural sources, such as fertilizer application, soil, and livestock, accounting for approximately 90% of the total global NH_3 emission,[12,16] which has dramatically increased by 80% from 1970 to 2017.[12]

Studies have been conducted to understand the formation mechanism and develop effective reduction strategies for NH_4NO_3 pollution. Some modeling studies have suggested that reduction of total NH_3 (TA) could be the most effective method to reduce PM concentrations.[9,17] For instance, Franchin *et al.* (2018) used ISORROPIA-II modeling showing that a reduction in the NH_3 concentration by approximately 50% could decrease the $PM_{1.0}$ concentration by ~36% in a rural area in Utah, United States. Moreover, in central China, which is surrounded by rural and urban areas, GEOS-Chem modeling results showed that a reduction in NH_3 emissions by 47% reduced the $PM_{2.5}$ concentrations by ~9% in July and ~11% in January.[17] By contrast, other modeling studies have shown that reducing NO_x emissions would be more effective than reducing NH_3 emissions for controlling PM.[18–20] Guo *et al.* (2018) showed that controlling NO_x emission would effectively reduce NO_3^- concentrations in an agricultural area in Cabauw, Netherlands. Furthermore, Chen *et al.* (2014) suggested that a 50% reduction in NO_x emissions would decrease $PM_{2.5}$ and NO_3^- concentrations by more than 24% and 42%, respectively, in an urban area in Bakersfield, USA. Analysis of ground-based data showed that NH_4NO_3 formation in the Salt Lake Valley is likely to be total HNO_3 (TN)-limited, and, thus, reduction of NO_x is effective in improving the air quality.[20] However, scientific data on highly efficient control strategies of

precursor gas in alleviating particulate NO_3^- in different areas are still lacking.

In this study, to determine NH_4NO_3 formation and related PM pollution conditions, two intensive field measurements of NH_3, NO_2, HNO_3, and water-soluble inorganic ions (WSIIs) in $PM_{1.0}$ were performed in the summer in Gimje, a rural area in South Korea. Gimje is a highly dense livestock area with populated livestock facilities and farms.[21] Extremely high NH_3 emission[22] and PM pollution[23] have been reported in this region. There are almost no studies on the temporal distribution of WSIIs and their precursor gases. In this study, the WSIIs and inorganic gas-particle-phase partitioning of NH_4NO_3 were analyzed by exploring the WSIIs and inorganic gases. Based on the measurement dataset and thermodynamic model ISORROPIA-II, we discuss the effective implementation of PM and NO_3^- reduction strategies in livestock-dense areas. Moreover, we compared the results acquired from the rural area with those from a nearby urban area, Jeonju, *via* thermodynamic modeling by using the NH_3 and WSII concentrations in $PM_{2.5}$ data measured from May 2019 to April 2020 by Park *et al.* (2021).[8]

Methods

Measurements

Particulate WSIIs and inorganic gases were measured in Gimje, Jeollabuk-do, South Korea (35.8395° N, 126.9889° E) (Fig. 1). The monitoring site has livestock complexes for raising pigs and chickens and large-scale farms with open manure storage facilities,[21,24] resulting in high NH_3 emissions.[22]

Two intensive field measurements were performed during the summer (June to July 2020) and winter (January to February 2021). In the livestock area, concentrations of inorganic gases such as NH_3, NO_x (NO, and NO_2), and HNO_3, and WSIIs in $PM_{1.0}$ (Na^+, NH_4^+, Mg^{2+}, Ca^{2+}, K^+, NO_3^-, SO_4^{2-}, and Cl^-) were measured. Atmospheric NH_3 was measured every 1 s using a real-time NH_3 instrument (DLT-100, Los Gatos Research, USA) using off-axis integrated cavity output spectroscopy. In principle, the NH_3 instrument using specific wavelengths does not require external calibration.[25] However, we performed calibration to confirm the performance of the instrument by mixing standard NH_3 (9.2 ppm, with an accuracy of ±2%, Air Korea, Korea) and N_2 (99.999%, Air Korea, Korea) gases before and after field measurements, resulting in an R^2 of 0.9999 (Fig. S1†). The detailed procedure for the calibration and measurement of atmospheric NH_3 is described by Park *et al.* (2021). For the analysis, we used hourly averaged concentrations of atmospheric NH_3. The NO_x concentration was also monitored every 1 m using a NO_x instrument (Serinus 40 Oxides of Nitrogen, Ecotech, Australia), based on the chemiluminescence method. Before and after conducting the field measurements, calibration was conducted by mixing standard NO (4.9 ppm, with an accuracy of ±10%, Air Korea, Korea) and N_2 (99.999%, Air Korea, Korea) gases at four different concentrations (20, 15, 12, and 0 ppb), which resulted in an error concentration of ~3%. The hourly averaged concentration of atmospheric NO_x was used for the analysis.
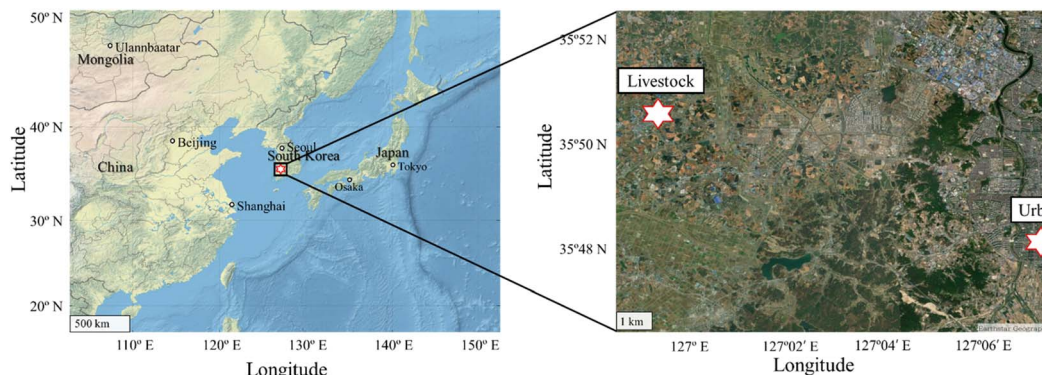
© 2023 The Author(s). Published by the Royal Society of Chemistry

Environ. Sci.: Atmos., 2023, **3**, 422–433 | **423**

Fig. 1 Map of the measurement site in livestock and urban areas, Jeollabuk-do, South Korea.

PM$_{1.0}$ and HNO$_3$ were collected using a two-stage sequential air sampler (APM Engineering, PMS-114, Korea) which has been widely used.[26,27] The sequential air sampler consisted of two stages for collection of PM$_{1.0}$ on a Teflon filter (PTFE, 66155, PALL, USA) at the first stage, and of HNO$_3$ on a nylon filter (Nylon, 1213776, GVS, USA) at the second stage. It was operated at a flow rate of 16.7 L min^{-1} for 24 h from 00:00 am to 00:00 am the following day during the measurement period. During the sampling, some semi-volatile species (i.e. NO$_3^-$, NH$_4^+$ and HNO$_3$) could be evaporated, leaving approximately ~10% of their total mass on the filters.[28,29] A total of 84 samples for PM$_{1.0}$ (42 samples) and HNO$_3$ (42 samples) were collected during all measurements. Subsequently, all filter samples were stored at −4 °C in a freezer and then analyzed within two weeks after collection. The PM$_{1.0}$ mass concentration collected from the Teflon filter was observed based on the procedure of the method of the USA Environmental Protection Agency.[30] To analyze the HNO$_3$ and WSIIs of PM$_{1.0}$, each filter sample was extracted in purified water (18.2 MΩ cm, Merck Milli-Q®, Millipore, Burlington, MA, USA). A detailed extraction procedure was described previously.[31] The extracts from nylon filters were analyzed to quantify the concentration of HNO$_3$, and the extracts from Teflon filters were analyzed to determine five cations (Na$^+$, NH$_4^+$, Mg^{2+}, Ca^{2+}, and K$^+$) and three anions (NO$_3^-$, SO$_4^{2-}$, and Cl$^-$) using ion chromatography (Aquion, Thermo Scientific, USA). The method detection limits (MDLs) of Na$^+$, NH$_4^+$, Ca^{2+}, Mg^{2+}, K$^+$, NO$_3^-$, SO$_4^{2-}$, and Cl$^-$ were 0.01, 0.01, 0.03, 0.01, 0.02, 0.02, 0.03 and 0.02 μg m^{-3}, respectively. For gaseous species, the MDLs of HNO$_3$, NO$_x$, and NH$_3$ were 0.01, 0.4,[32] and 0.5 (ref. 25) ppb, respectively. Hourly averaged meteorological parameters, including relative humidity (RH), temperature, wind direction, precipitation, and wind speed, were obtained during the measurement period from the Korea Meteorological Administration in Jeonju.[33]

Thermodynamic modeling

To estimate whether HNO$_3$ or NH$_3$ is the limiting factor for particulate NO$_3^-$ formation and to calculate aerosol liquid water content (ALWC), we used ISORROPIA-II, an extensively applied thermodynamic equilibrium model based on a Na$^+$–Cl$^-$–Ca^{2+}– K$^+$–Mg^{2+}–SO$_4^{2-}$–NH$_4^+$–NO$_3^-$–H$_2$O aerosol system.[18,34,35] As model inputs, the measured concentrations of TA (particle-phase NH$_4^+$ + gas-phase NH$_3$), TN (particle-phase NO$_3^-$ + gas-phase HNO$_3$), Na$^+$, K$^+$, Ca^{2+}, Mg^{2+}, Cl$^-$, and SO$_4^{2-}$ and meteorological parameters in the rural area were used. ALWC was also calculated using measured data of inorganic gases, WSIIs, temperature, and RH.[35] It was reported that a correlation coefficient between the simulated ISORROPIA-II ALWC and the measured hygroscopic growth factors agreed well at ~0.89; however, the uncertainty of the predicted ALWC in aerosols would be ~20% compared to the observed ALWC.[36] This underestimation might be due to the unidentified organic species information in ISORROPIA-II.[35,36]

In this study, we used the "forward" mode, which calculates gas-particle equilibrium partitioning concentrations using the total concentration of species because this mode provides substantially better computational results for the concentrations of inorganic gases than the reverse mode.[18,37] The mean RH of 74.7 ± 11.3% observed throughout the monitoring site was below the deliquescence relative humidity (DRH) for pure (NH$_4$)$_2$SO$_4$.[4] However, PM$_{1.0}$ could still absorb water below the DRH of the pure salt because PM is a complex mixture of various inorganic salts and organic compounds.[37–39] Therefore, we used the "metastable state" solution, assuming that the aerosol compositions are an aqueous supersaturated solution that prevents the formation of a solid precipitate.[35,37]

To compare the phenomena of gas-particle partitioning between rural and urban areas, we also calculated the limiting factor of particulate NO$_3^-$ formation and gas-particle partitioning using previous data (measured from May 2019 to April 2020) of WSIIs in PM$_{2.5}$ and NH$_3$ measured in Jeonju, an urban area situated approximately 10 km from Gimje.[8] In this study, HNO$_3$ measurement data were unavailable for the urban area; thus, the concentration was estimated using the method of Seo et al. (2020).[40] The uncertainty in the estimated TN was confirmed by comparing the measured TN at the rural site (Fig. S2†). To confirm the thermodynamic equilibrium, we also compared the measured and predicted values of the SNA (SO$_4^{2-}$, NO$_3^-$, NH$_4^+$) species (Fig. S1 and S3†). Fig. S3† shows the scatter plots of observations against model predictions of

the major secondary inorganic aerosol (SIA) species (NH_4^+, NO_3^- and SO_4^{2-}) in livestock and urban areas during measurement periods. A good correlation was found between observations and model predictions, suggesting the good performance of ISORROPIA-II.

Conditional probability function (CPF) analysis

To identify the potential regional-scale transport and local emission sources, a conditional probability function (CPF) analysis was conducted using the wind direction, wind speed, and NH_3 and NO_2 concentrations. The CPF estimates a probability that the given source contribution from the given wind speed and wind direction will exceed a threshold criterion. The threshold criterion was set at the 80th percentile to indicate the directionality of the source.

Results and discussion

Overview of gaseous species and WSIIs

Two intensive measurements of inorganic gaseous species (namely, HNO_3, NO, NO_2, and NH_3) and WSIIs in $PM_{1.0}$ were conducted in the highly dense livestock area of Gimje during the summer and winter of 2020–2021. Fig. 2 shows the daily averaged variations in meteorological parameters, gaseous species, and WSIIs in $PM_{1.0}$. Over the study period, the daily average temperature was 15.1 ± 9.8 °C, and RH was $74.7 \pm 11.3\%$ (Fig. 2A). The mean concentrations of NH_3, HNO_3, NO, and NO_2 were 96.9, 0.7, 2.3, and 21.3 ppb, respectively (Fig. 2B). The atmospheric NH_3 concentration in the populated livestock area was significantly (2–35 times) higher than that in other livestock and urban areas listed in Table 1.[8,27,41–45] This is because of livestock activities, open manure storage facilities, and livestock waste disposal in the region. The HNO_3 concentration at the monitoring site was lower than that reported in

Seoul,[27] Quzhou, Beijing,[41] and New Delhi[42] but higher than that reported in Jeonju,[8] Seolseongmyeon,[27] Gucheng,[43] Niangon Adjamé[44] and San Diego[45] (Table 1).

The daily concentrations of $PM_{1.0}$ and its WSIIs are shown in Fig. 2C. The daily averaged $PM_{1.0}$ mass concentration ranged from 3.3 to 45.2 µg m^{-3}, with an average of 20.1 ± 8.8 µg m^{-3}. NO_3^-, SO_4^{2-}, and NH_4^+ were the major components of $PM_{1.0}$, and the daily concentration of NO_3^- ranged from 0.4 to 22.0 µg m^{-3} with an average of 4.8 ± 3.9 µg m^{-3}. The daily SO_4^{2-} concentrations fluctuated between 0.1 and 7.1 µg m^{-3}, with an average of 3.5 ± 1.8 µg m^{-3}. The daily NH_4^+ concentrations varied from 0.2 to 9.4 µg m^{-3} and showed an average of 2.8 ± 1.6 µg m^{-3}. Among all WSII species, a significant dominance of NO_3^- was observed at the livestock site during the measurement period (Fig. 2C).

All WSIIs, $PM_{1.0}$, and inorganic gaseous species, except for SO_4^{2-} and HNO_3, exhibited higher concentrations in the winter (Table S1†). Among the WSIIs, the NO_3^- concentration was remarkably enhanced from 2.9 µg m^{-3} in the summer to 7.3 µg m^{-3} in the winter (Table S1 and Fig. S4E†). However, the HNO_3 concentration dramatically decreased to an average of 0.1 ppb in the winter (summer: 1.1 ppb) (Table S1 and Fig. S4C†). Theoretically, NH_3 and HNO_3 phases are dependent on temperature and RH.[4] NH_4NO_3 partitions can occur from the particle-phase to the gas-phase at low RH and high temperature.[4,46] For this reason, NO_3^- is mostly present in gaseous HNO_3 during the summer and has low concentrations, whereas NO_3^- is partitioned into particle-phase NO_3^- during the winter, resulting in higher atmospheric NO_3^- concentrations. Our results, which revealed low HNO_3 levels in the summer and high NO_3^- levels in the winter, are consistent with previously reported ones.[27,47] NH_3 is generally temperature-dependent. Thus, high NH_3 levels have been reported in the summer.[8,27,48] However, the atmospheric NH_3
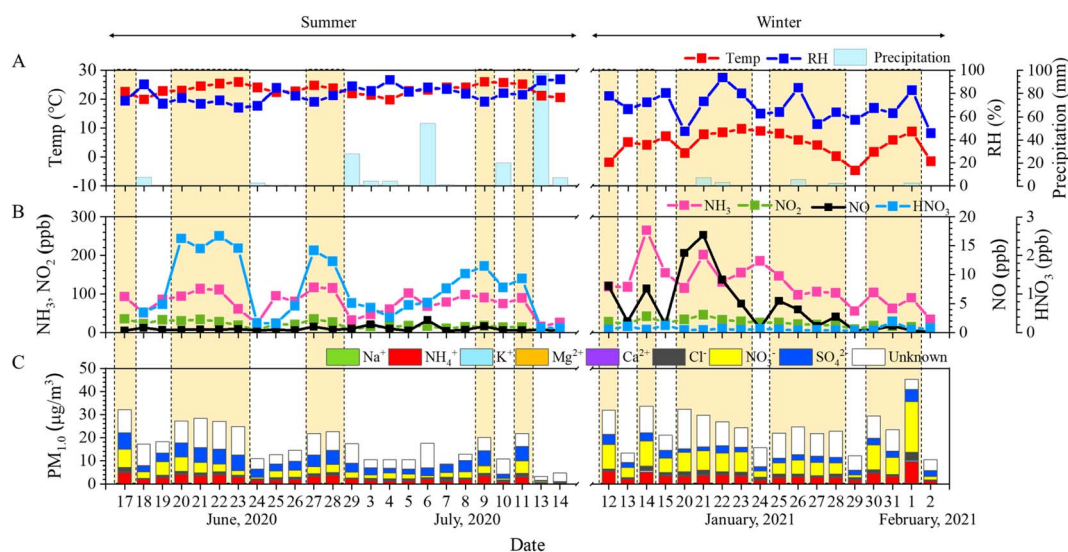

Fig. 2 Daily averaged variations in (A) temperature (temp.), relative humidity (RH), and precipitation, (B) NH_3, NO_2, NO, and HNO_3 concentrations, and (C) water-soluble ions in $PM_{1.0}$ in the livestock area during the measurement period. The light-yellow shadows represent $PM_{1.0}$ pollution days ($PM_{1.0} \geq 20$ µg m^{-3}).

© 2023 The Author(s). Published by the Royal Society of Chemistry

Environ. Sci.: Atmos., 2023, **3**, 422–433 | **425**

Table 1 List of atmospheric average NH_3 and HNO_3 concentrations in various environments

Location	Period	NH_3 (unit: ppb)	HNO_3 (unit: ppb)	References
Livestock area				
Gimje, Korea	2020.6–2020.7 2021.1–2021.2	96.9	0.7	This study
Seolseongmyeon, Korea	2009.1–2018.12	50.0	0.4	Sung et al. (2020)[27]
Quzhou, China	2011.1–2014.12	31.2	2.7	Xu et al. (2016)[41]
Gucheng, China	2013.5–2013.9	36.2	0.2	Meng et al. (2018)[43]
Niangon Adjamé, Côte d'Ivoire	2015.12–2016.2	44.0	0.2	Bahino et al. (2018)[44]
Urban area				
San Diego, United States	2007.2–2012.3	3.3	0.2	Li et al. (2014)[45]
Seoul, Korea	2009.1–2018.12	7.5	0.7	Sung et al. (2020)[27]
Beijing, China	2011.1–2014.12	17.2	3.2	Xu et al. (2016)[41]
New Delhi, India	2017.12–2018.2	33.9	1.0	Acharja et al. (2020)[42]
Jeonju, Korea	2019.5–2020.4	10.5	0.2[a]	Park et al. (2021)[8]

[a] Estimation based on an equation from Seo et al., 2020.

concentration was significantly higher in the winter (124.6 ppb) than in the summer (76.0 ppb) (Table S1 and Fig. S4D†). The plausible reasons for this observation are (1) active manure production at the open storage from the livestock farms and (2) dense NH_3 emissions from mechanically ventilated farms with a low ventilation rate in winter in the study area.[31] Higher NH_3 concentrations have been reported previously in the winter than in other seasons in livestock areas.[31,49]

Enhancements of nitrate during PM pollution

To investigate the phenomenon of $PM_{1.0}$ pollution in the livestock area, we compared the chemical characteristics of $PM_{1.0}$ on clean and pollution days. Based on $PM_{1.0}$ mass concentrations, we classified days into clean (daily average $PM_{1.0} < 20$ µg m^{-3}) and pollution days (daily average $PM_{1.0} \geq 20$ µg m^{-3}), as suggested in previous studies.[50,51] On clean days, the average concentration of $PM_{1.0}$ was 12.1 ± 4.0 µg m^{-3}, and WSIIs accounted for 58.2% (7.1 µg m^{-3}) of $PM_{1.0}$ (Fig. 3A). SO_4^{2-} was
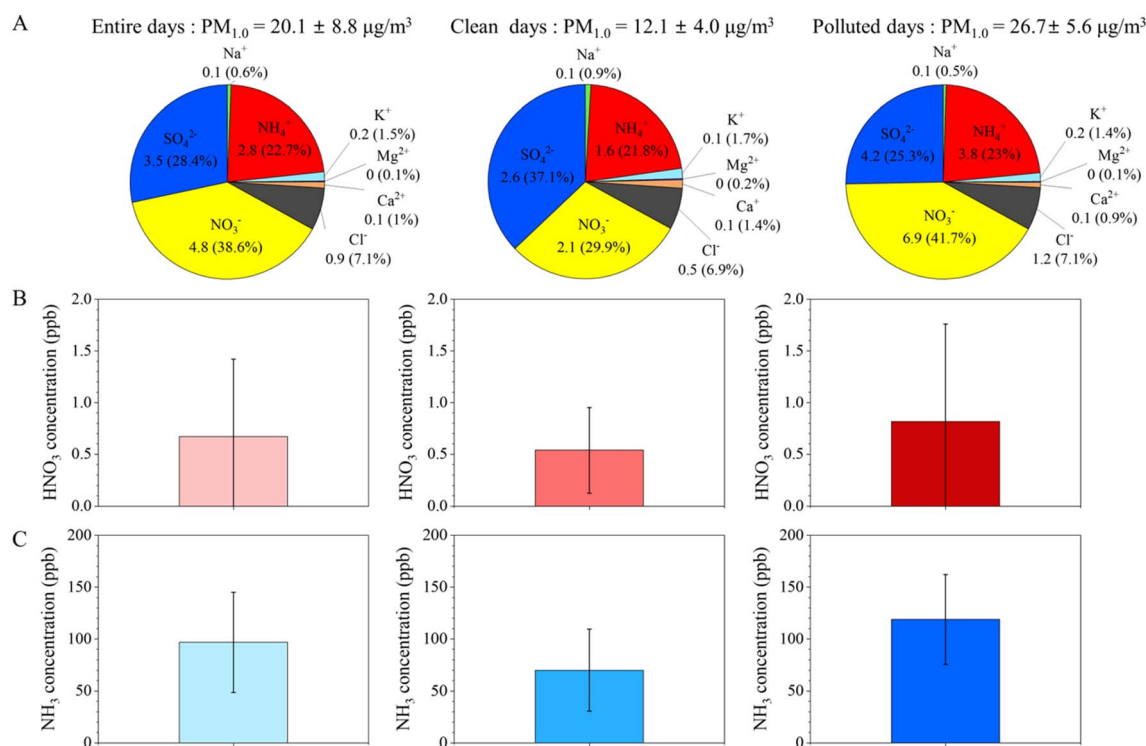

Fig. 3 Comparison of (A) water-soluble ions in $PM_{1.0}$, (B) HNO_3 concentration, and (C) NH_3 concentrations for entire, clean ($PM_{1.0} < 20$ µg m^{-3}), and high pollution ($PM_{1.0} \geq 20$ µg m^{-3}) days.
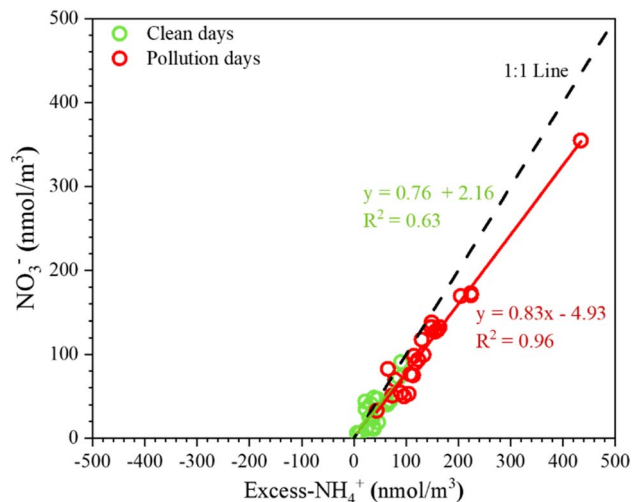
Fig. 4 Scatter plot of molar concentrations of NO_3^- and excess-NH_4^+ in the livestock area during clean and pollution days. The green and red lines represent the regression of the clean and pollution days, respectively.

the most dominant ion during the clean days, accounting for 37.1% of $PM_{1.0}$, followed by NO_3^- (29.9%) and NH_4^+ (21.8%). Out of 42 days, 23 were defined as $PM_{1.0}$-pollution days at the monitoring site. During pollution days, the daily averaged concentration of $PM_{1.0}$ was 26.7 ± 5.6 μg m^{-3} with a remarkably enhanced NO_3^- fraction (41.7%) in $PM_{1.0}$ (Fig. 3A), followed by SO_4^{2-} (25.3%) and NH_4^+ (23.0%). Moreover, the daily average concentrations of NH_3 and HNO_3 increased significantly to 118.9 ppb and 0.8 ppb, respectively, during pollution days when

NO_3^- molar concentrations showed a significant correlation, with a slope close to 1.0, thereby indicating that the formation of NH_4NO_3 was primarily through the reaction between NH_3 and HNO_3. This is because of the extremely high levels of atmospheric NH_3 at the livestock site during the study period.[52] Moreover, a shallower slope for both clean (0.76) and pollution (0.83) days was observed for a livestock site, indicating that most of the measured $PM_{1.0}$ samples were residual NH_4^+ associated with species other than NO_3^-, such as ammonium chloride (NH_4Cl). This implies that there is enough excess NH_4^+ that it can drive the partitioning of other semi-volatile acids such as HNO_3 and HCl.[53]

HNO_3/NH_3 limitation of particulate nitrate formation

In the livestock area, PM pollution with a drastic enhancement of NO_3^- occurred under NH_3-rich conditions, indicating that both NH_3 and HNO_3 are critical precursors for $PM_{1.0}$ nitrate formation. To suggest a reduction of such high NO_3^- concentrations in the livestock area, we calculated the limiting factor for NO_3^- formation using the ISORROPIA-II model.[35,54] The measurement data of the average WSII concentrations, temperature, and RH were used as the model input data (Table S1†).

Fig. 5A shows the contour plots of simulated NO_3^- concentrations depending on the TA and TN levels at the minimum SO_4^{2-} (~1 μg m^{-3}) and maximum SO_4^{2-} (~10 μg m^{-3}) concentrations, respectively. In this figure, the left side is the TA-limited area and the right side is the TN-limited area, which were calculated using eqn (1) (unit of each species: μmol m^{-3}) as follows:[55]

$$R = \frac{TA}{2SO_4^{2-} + NO_3^- + HNO_3 + Cl^- + HCl^- - 2Ca^{2+} - Na^+ - K^+ - 2Mg^{2+}} \qquad (1)$$

compared with those during clean days (70.1 ppb and 0.5 ppb, respectively) (Fig. 3B and C). These findings suggest that NH_3 and HNO_3 play a critical role in NO_3^- formation during high-$PM_{1.0}$ events.

Fig. S5† illustrates the CPF result during pollution days. A high probability of NH_3 concentration (179 ppb at the 80th percentile) was observed around the measurement site during pollution days, suggesting that the high levels of NH_3 were mostly affected by local sources around the livestock complexes rather than long-range transport.

$PM_{1.0}$ nitrate formation

Fig. 4 shows the relationship between NO_3^- and excess-NH_4^+ molar concentrations. The excess-NH_4^+ concentration ranged from 6.0 to 434.3 nmol m^{-3}, and NO_3^- molar concentrations increased with excess-NH_4^+ molar concentrations during both clean and pollution days, supporting that NO_3^- formation always occurred at the monitoring site. The excess-NH_4^+ and

The measurement data of TA and TN during clean (black circles) and pollution days (pink circles) are shown in Fig. 5. All measured data were TN-limited on both clean and pollution days in all cases of minimum and maximum SO_4^- concentrations, given the NH_3-rich concentration in the study area (Fig. 5A). NO_3^- formation in livestock can be controlled through HNO_3. Hence, to reduce HNO_3 concentrations, controlling NO_x emissions might be an important approach to reduce NO_3^- concentrations and thus improve air quality in livestock areas.

Park *et al.* (2021) observed remarkable NH_4NO_3 formation during high $PM_{2.5}$ events at nearby urban sites. To compare the results of the limiting factor for NO_3^- formation in an urban area, we calculated the limiting factor in Jeonju, a nearby urban area, using measurement data from May 2019 to April 2020.[8] The method and procedure applied for ISORROPIA-II simulation were used for this step as well. The measurement values of the WSIIs in $PM_{2.5}$, NH_3, temperature, and RH in the nearby urban area were used as the input data (Table S1†);[8] however,

Environmental Science: Atmospheres
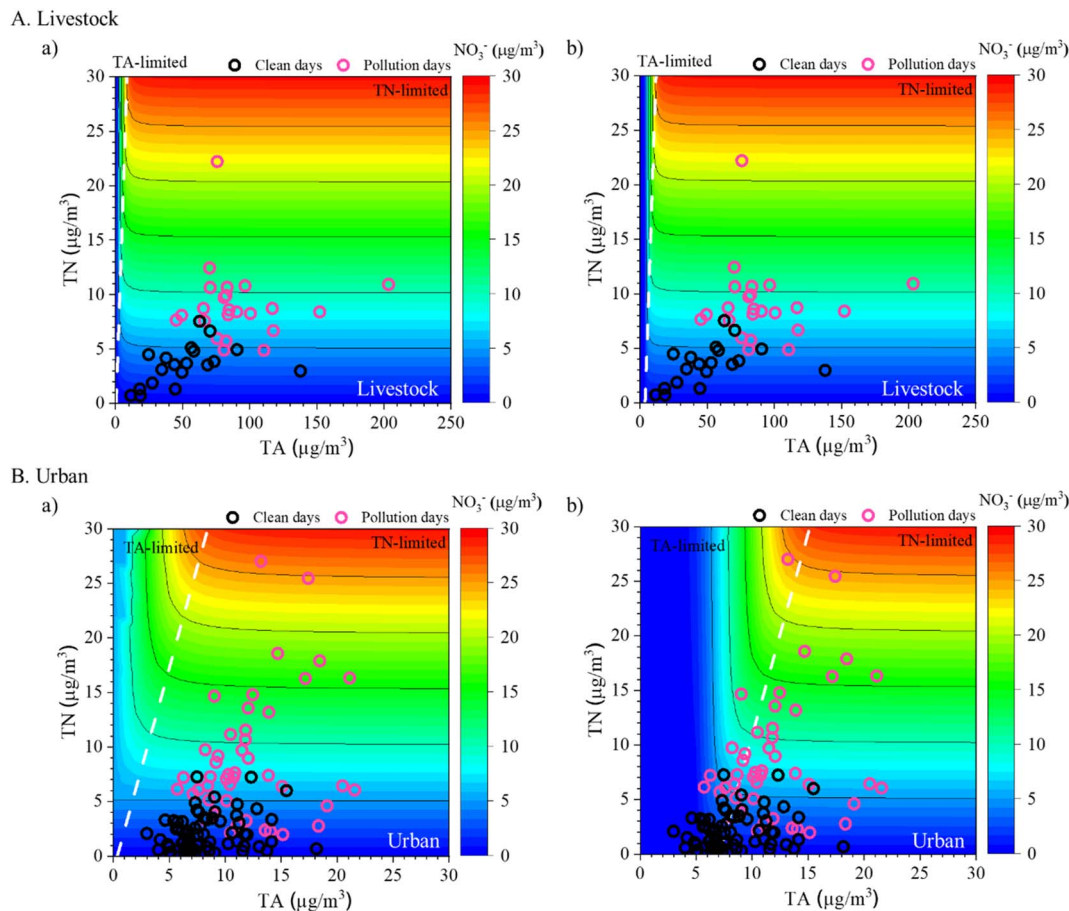
View Article Online

Paper

Fig. 5 NO_3^- concentrations calculated using the ISORROPIA-II model depending on total nitrate (TN) and total ammonia (TA) concentrations under (a) $SO_4^{2-} = 1\ \mu g\ m^{-3}$ and (b) $SO_4^{2-} = 10\ \mu g\ m^{-3}$ in the (A) livestock area and under (a) $SO_4^{2-} = 1\ \mu g\ m^{-3}$ and (b) $SO_4^{2-} = 20\ \mu g\ m^{-3}$ in (B) the urban area[8] during clean and pollution days. Measurement data of TN and TA concentrations during the monitoring periods are shown by black circles (clean days) and pink circles (pollution days).

the HNO_3 concentration was estimated using ISORROPIA-II because of the absence of data (details are given in S1 in the ESI†). The simulation results showed that under low-SO_4^{2-} conditions (~1 $\mu g\ m^{-3}$), all observed data were affected by the TN-limited regime on both clean and pollution days in the urban area (Fig. 5B). In contrast, although under high-SO_4^{2-} (~20 $\mu g\ m^{-3}$), the measured data fell into both TA-limited and TN-limited regimes during clean days, and most of the data fell into the TN-limited regime during pollution days (Fig. 5B). As the daily SO_4^{2-} concentration in the urban area was ~4.3 $\mu g\ m^{-3}$, the TN-limited regime was more reliable in most cases. This shows that high NO_3^- production in the urban area during $PM_{2.5}$-pollution days was also mainly controlled by HNO_3. Therefore, to alleviate particulate NO_3^- in PM in both livestock and nearby urban areas, control of NO_x emissions (which reduces the HNO_3 concentration) could be crucial.

The efficiency of PM reduction *via* precursor controls

To understand the alleviating efficiency of particulate NO_3^- in PM in livestock and urban areas, we performed a sensitivity analysis using ISORROPIA-II, for which the measurement-

averaged data were used as input data (Table S1†). Given the abundance of inorganic salts in both areas, we assumed that the $SO_4^{2-}-NH_4^+-NO_3^--H_2O$ system is in equilibrium and that particulate NO_3^- is formed through the gas-particle partitioning of NH_3 and HNO_3.

First, we attempted to control the TN concentration to study the decrease in particulate NO_3^- and PM concentrations caused by HNO_3 reduction in both livestock and urban areas. In Korea, HNO_3 and NO_x are mainly locally contributed rather than long-range transported to form a particle-phase given their lifetimes and concentrations.[56] During the measurement periods, the CPF results for NO_2 also showed a high probability of high NO_2 concentrations in both livestock and urban areas occurring locally, supporting that the high NO_2 concentration originated near the study area rather than during long-range transport (Fig. S6†).

Fig. 6 shows the sensitivity results for TN control in livestock and urban areas. The PM mass concentrations decreased linearly as TN decreased in both livestock and urban areas (Fig. 6A and B). In the livestock area, a 50% decrease in the TN resulted in a 50% decrease in the particulate NO_3^- and an approximately 33% decrease in the $PM_{1.0}$ mass concentrations during the
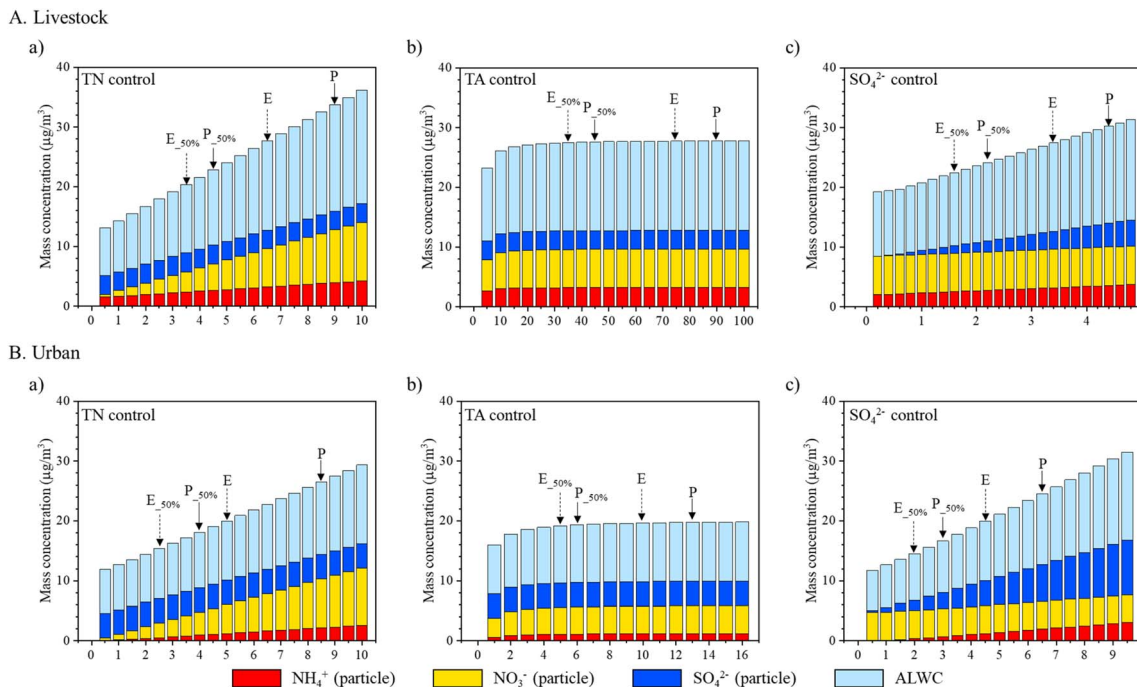
428 | *Environ. Sci.: Atmos.*, 2023, **3**, 422–433 © 2023 The Author(s). Published by the Royal Society of Chemistry

Fig. 6 Thermodynamic ISORROPIA-II model simulations for SO_4^{2-}, NO_3^-, and NH_4^+ (SNA) concentrations and aerosol liquid water content (ALWC) varied by (a) total nitrate (TN), (b) total ammonia (TA) and (c) SO_4^{2-} concentration inputs in (A) livestock and (B) urban areas. "E" indicates the wet particulate matter (PM) mass concentration during entire days and "P" indicates the wet PM mass concentration during pollution days. "$E_{-50\%}$" and "$P_{-50\%}$" indicate the wet PM mass concentration when TN, TA, and SO_4^{2-} are reduced by up to 50%. The following inputs were used in the model: temperature (livestock: 288.3 K; urban: 288.2 K); relative humidity (livestock: 75%; urban: 64%); and TN, TA, and SO_4^{2-} concentrations (livestock: 6.5, 73.1, and 3.5 µg m^{-3}; urban: 4.8, 9.9, and 4.4 µg m^{-3}) (Table S1†).

entire period as well as during pollution periods (Fig. 6A). Significant responses in NO_3^- (50%) and $PM_{2.5}$ (~23%) were observed during an entire day in the urban area, but a higher reduction in NO_3^- (50%) and $PM_{2.5}$ (31%) was predicted by a 50% decrease in the TN during pollution days (Fig. 6B). Therefore, to decrease particulate NO_3^- and PM concentrations in both areas, controlling HNO_3 is a highly efficient approach.

Second, a sensitivity analysis was performed by controlling TA (Fig. 6). Atmospheric NH_3 is generally considered a local contributor because of its short lifetime.[57] As shown in Fig. 6A and B, a 50% decrease in TA did not respond to the NO_3^- and PM concentrations (only ~1% in the livestock site and ~2% in the urban site). An ~87% (livestock) and ~78% (urban) reduction in TA would be required to effectively decrease PM mass concentrations.

Finally, SO_4^{2-} was controlled during the simulation. SO_4^{2-} does not undergo gas-particle partitioning and is favored in the particle-phase because of its low volatility.[4] Reportedly, SO_2 can be transported from China to Korea, and therefore, we cannot rule out the possibility of the transported SO_4^{2-}.[58]

Illustrated in Fig. 6A and B are the results of SO_4^{2-} control in the two regions. If we assume that SO_4^{2-} is not transported at all to the receptor areas and formed locally by applying to the actual measured concentration of SO_4^{2-} (livestock: 3.5 µg m^{-3} and urban: 4.3 µg m^{-3}), only the PM concentration can be found to decrease in the livestock ($PM_{1.0}$: ~20%, NO_3^-: ~0.1%, Fig. 6A) and urban areas ($PM_{2.5}$: ~30%, NO_3^-: ~0.0%, Fig. 6B)

during PM pollution. A similar reduction in PM was observed during the entire period in both areas. However, some SO_4^{2-} may have been transported from outside Korea. A modeling study showed that approximately half of the SO_4^{2-} in $PM_{2.5}$ was transported from China to South Korea during 2012–2016.[58] Accordingly, if we assume that only half of the SO_4^{2-} was locally produced, then a 50% reduction in SO_4^{2-} leads to a reduction in the $PM_{1.0}$ and $PM_{2.5}$ concentrations in the livestock ($PM_{1.0}$: ~12%, NO_3^-: ~0.1%, Fig. 6A) and urban areas ($PM_{2.5}$: ~20%, NO_3^-: ~0.0%, Fig. 6B) during PM pollution. On an entire day, a 50% decrease in the SO_4^{2-} concentration could lead to a ~13% decrease in PM concentrations and ~0.0% decrease in the particulate NO_3^- concentration in the livestock and urban areas. For SO_4^{2-} control, a linear reduction in the SO_4^{2-} concentration, regardless of whether SO_4^{2-} was transported, resulted in a linear decrease in PM mass concentrations but a non-linear decrease in the particulate NO_3^- concentration.

Additionally, we investigated the effect of TN, TA, and SO_4^{2-} control on the gas-particle partitioning of HNO_3 and NH_3. Almost ~96% of the TA remains in the gas-phase in a livestock area when the TN, TA, and SO_4^{2-} were reduced (Fig. S7A, S8A, and S9A†); however, a decrease in the TN and SO_4^{2-} led to more evaporation of particulate NH_4^+ into more gaseous NH_3 in an urban area (Fig. S7B and S9B†). However, the particle-phase of NO_3^- was always the dominant form in both sites (Fig. S7–S9†).

Conclusions

We monitored NH_3, HNO_3, and WSII concentrations in $PM_{1.0}$, in a livestock area in Gimje, from June to July 2020 and January to February 2021 to characterize NO_3^- formation. During the study periods, the average concentrations of NH_3 and HNO_3 were 96.9 and 0.7 ppb, respectively, and the daily average of $PM_{1.0}$ concentration was 20.1 $\mu g\ m^{-3}$, with averages of 2.8 $\mu g\ m^{-3}$ for NH_4^+, 4.8 $\mu g\ m^{-3}$ for NO_3^-, and 3.5 $\mu g\ m^{-3}$ for SO_4^{2-}. On pollution days ($PM_{1.0} \geq 20\ \mu g\ m^{-3}$), a remarkable increase in the fraction of NO_3^- in $PM_{1.0}$ and the daily NH_3 and HNO_3 concentrations was observed, suggesting the critical role of NH_3 and HNO_3 in NO_3^- formation. The measurements and ISORROPIA-II-simulated results showed that NO_3^- formation in the livestock area was always TN-limited owing to its NH_3-rich environment. Recent studies showed that some amount of the water content of organic materials ($\sim$30%) could influence the water content and pH of aerosol particles.[36,59] Further studies are needed to confirm the effect of organic materials on aerosol water content. Recent studies reported that VOC reduction would be efficient in reducing NH_4NO_3 aerosol in some areas.[60–62] To confirm this, further studies are needed with more measurement datasets.

In comparing the effect of reducing particulate NO_3^- and PM concentrations by controlling TN, TA, and SO_4^{2-} from two different environments (i.e., livestock and urban areas), we found that reducing TN is more effective than reducing TA and SO_4^{2-} in alleviating particulate NO_3^- and PM in both areas. Collectively, our results provide an understanding of the characteristics and formation of NO_3^-—the most serious aerosol pollutants in Korea—as well as provide scientific data to develop effective PM reduction policies for livestock and urban areas.

Author contributions

M. S. designed this study. H. K., J. P., S. G. K. and M. S. conducted measurements and analysed the data. M. S., H. K., K. P. and S. G. K prepared the manuscript.

Conflicts of interest

There are no conflicts to declare.

Acknowledgements

Notes and references

1 B. B. Booth, N. J. Dunstone, P. R. Halloran, T. Andrews and N. Bellouin, Aerosols implicated as a prime driver of twentieth-century North Atlantic climate variability, Nature, 2012, 484, 228–232, DOI: 10.1016/j.envint.2016.02.003.

2 G. Bhattarai, J. B. Lee, M.-H. Kim, S. Ham, H.-S. So, S. Oh, H.-J. Sim, J.-C. Lee, M. Song and S.-H. Kook, Maternal exposure to fine particulate matter during pregnancy induces progressive senescence of hematopoietic stem cells under preferential impairment of the bone marrow microenvironment and aids development of myeloproliferative disease, Leukemia, 2020, 34, 1481–1484, DOI: 10.3390/ijerph14040440.

3 G. Myhre, D. Shindell and F. M. Breon, Anthropogenic and natural radiative forcing, in IPCC, Climate Change 2013: The Physical Science Basis, Working Group I Contribution to the IPCC Fifth Assessment Report, https://www.ipcc.ch/report/ar5/wg1/anthropogenic-and-natural-radiative-forcing/, accessed on 1 April 2022.

4 J. Seinfeld and S. Pandis, Atmospheric Chemistry and Physics: From Air Pollution to Climate Change, Wiley, Hoboken, NJ, USA, 3rd edn, 2016, ISBN 978-1-118-94740-1.

5 J. L. Jimenez, M. Canagaratna, N. Donahue, A. Prevot, Q. Zhang, J. H. Kroll, P. F. DeCarlo, J. D. Allan, H. Coe and N. Ng, Evolution of organic aerosols in the atmosphere, science, 2009, 326, 1525–1529, DOI: 10.1126/science.1180353.

6 Z. Cheng, L. Luo, S. Wang, Y. Wang, S. Sharma, H. Shimadera, X. Wang, M. Bressi, R. M. de Miranda and J. Jiang, Status and characteristics of ambient $PM_{2.5}$ pollution in global megacities, Environ. Int., 2016, 89, 212–221, DOI: 10.1016/j.envint.2016.02.003.

7 Y.-C. Lin, Y.-L. Zhang, M.-Y. Fan and M. Bao, Heterogeneous formation of particulate nitrate under ammonium-rich regimes during the high-$PM_{2.5}$ events in Nanjing, China, Atmos. Chem. Phys., 2020, 20, 3999–4011, DOI: 10.5194/acp-20-3999-2020.

8 J. Park, E. Kim, S. Oh, H. Kim, S. Kim, Y. P. Kim and M. Song, Contributions of Ammonia to High Concentrations of $PM_{2.5}$ in an Urban Area, Atmosphere, 2021, 12, 1676, DOI: 10.3390/atmos12121676.

9 A. Franchin, D. L. Fibiger, L. Goldberger, E. E. McDuffie, A. Moravek, C. C. Womack, E. T. Crosman, K. S. Docherty, W. P. Dube and S. W. Hoch, Airborne and ground-based observations of ammonium-nitrate-dominated aerosols in a shallow boundary layer during intense winter pollution episodes in northern Utah, Atmos. Chem. Phys., 2018, 18, 17259–17276, DOI: 10.5194/acp-18-17259-2018.

10 S. S. Brown and J. Stutz, Nighttime radical observations and chemistry, Chem. Soc. Rev., 2012, 41, 6405–6447, DOI: 10.1039/C2CS35181A.

11 R.-J. Huang, J. Duan, Y. Li, Q. Chen, Y. Chen, M. Tang, L. Yang, H. Ni, C. Lin and W. Xu, Effects of NH_3 and alkaline metals on the formation of particulate sulfate and nitrate in wintertime Beijing, Sci. Total Environ., 2020, 717, 137190, DOI: 10.1016/j.scitotenv.2020.137190.

12 E. E. McDuffie, S. J. Smith, P. O'Rourke, K. Tibrewal, C. Venkataraman, E. A. Marais, B. Zheng, M. Crippa, M. Brauer and R. V. Martin, A global anthropogenic emission inventory of atmospheric pollutants from sector- and fuel-specific sources (1970–2017): an application of the

© 2023 The Author(s). Published by the Royal Society of Chemistry

Community Emissions Data System (CEDS), *Earth Syst. Sci. Data*, 2020, **12**, 3413–3442, DOI: **10.5194/essd-12-3413-2020**.

13 P. Oikawa, C. Ge, J. Wang, J. Eberwein, L. Liang, L. Allsman, D. Grantz and G. Jenerette, Unusually high soil nitrogen oxide emissions influence air quality in a high-temperature agricultural region, *Nat. Commun.*, 2015, **6**, 1–10, DOI: **10.1038/ncomms9753**.

14 M. Almaraz, E. Bai, C. Wang, J. Trousdell, S. Conley, I. Faloona and B. Z. Houlton, Agriculture is a major source of NO_x pollution in California, *Sci. Adv.*, 2018, **4**, eaao3477, DOI: **10.1126/sciadv.aao3477**.

15 X. Lu, X. Ye, M. Zhou, Y. Zhao, H. Weng, H. Kong, K. Li, M. Gao, B. Zheng and J. Lin, The underappreciated role of agricultural soil nitrogen oxide emissions in ozone pollution regulation in North China, *Nat. Commun.*, 2021, **12**, 1–9, DOI: **10.1038/s41467-021-25147-9**.

16 M. A. Sutton, S. Reis, S. N. Riddick, U. Dragosits, E. Nemitz, M. R. Theobald, Y. S. Tang, C. F. Braban, M. Vieno and A. J. Dore, Towards a climate-dependent paradigm of ammonia emission and deposition, *Philos. Trans. R. Soc., B*, 2013, **368**, 20130166, DOI: **10.1098/rstb.2013.0166**.

17 Z. Zhang, Y. Yan, S. Kong, Q. Deng, S. Qin, L. Yao, T. Zhao and S. Qi, Benefits of refined NH_3 emission controls on $PM_{2.5}$ mitigation in Central China, *Sci. Total Environ.*, 2022, **814**, 151957, DOI: **10.1016/j.scitotenv.2021.151957**.

18 H. Guo, R. Otjes, P. Schlag, A. Kiendler-Scharr, A. Nenes and R. J. Weber, Effectiveness of ammonia reduction on control of fine particle nitrate, *Atmos. Chem. Phys.*, 2018, **18**, 12241–12256, DOI: **10.5194/acp-18-12241-2018**.

19 J. Chen, J. Lu, J. C. Avise, J. A. DaMassa, M. J. Kleeman and A. P. Kaduwela, Seasonal modeling of $PM_{2.5}$ in California's San Joaquin Valley, *Atmos. Environ.*, 2014, **92**, 182–190, DOI: **10.1016/j.atmosenv.2014.04.030**.

20 R. Kuprov, D. J. Eatough, T. Cruickshank, N. Olson, P. M. Cropper and J. C. Hansen, Composition and secondary formation of fine particulate matter in the Salt Lake Valley: Winter 2009, *J. Air Waste Manage. Assoc.*, 2014, **64**, 957–969, DOI: **10.1080/10962247.2014.903878**.

21 Korean Statistical Information Service (KOSIS), **https://kosis.kr**, accessed on 1 April 2022.

22 Clean Air Policy Support System (CAPSS). *2017 Korea National Air Pollutants Emission*. 2019, **https://airemiss.nier.go.kr**, accessed on 1 April 2022.

23 C. Han, S. Kim, Y.-H. Lim, H.-J. Bae and Y.-C. Hong, Spatial and temporal trends of number of deaths attributable to ambient $PM_{2.5}$ in the Korea, *J. Korean Med. Sci.*, 2018, **33**, 1–14, DOI: **10.3346/jkms.2018.33.e193**.

24 J.-S. Hwang, Y.-K. Park and C.-H. Won, Runoff characteristics of non-point source pollution in lower reaches of livestock area, *J. Korean Soc. Environ. Eng.*, 2012, **34**, 557–565, DOI: **10.4491/KSEE.2012.34.8.557**.

25 ABB, ABB-Los Gatos Research Inc., *Off-Axis Integrated Cavity Output Spectroscopy (OA-ICOS)*, **http://www.lgrinc.com/advantages/**, accessed on 1 April 2022.

26 E. S. Edgerton, Y.-M. Hsu, E. M. White, M. E. Fenn and M. S. Landis, Ambient concentrations and total deposition of inorganic sulfur, inorganic nitrogen and base cations in the Athabasca Oil Sands Region, *Sci. Total Environ.*, 2020, **706**, 134864, DOI: **10.1016/j.scitotenv.2019.134864**.

27 M. Sung, J. Park, J. Lim, H. Park and S. Cho, A long term trend of gaseous and particulate acid/base species and effects of ammonia reduction on nitrate contained in $PM_{2.5}$, 2009∼ 2018, *J. Korean Soc. Atmos*, 2020, **36**, 249–261, DOI: **10.5572/KOSAE.2020.36.2.249**.

28 C. J. Tsai, C. H. Huang and H. H. Lu, Adsorption capacity of a nylon filter of filter pack system for HCl and HNO_3 gases, *Sep. Sci. Technol.*, 2005, **39**, 629–643, DOI: **10.1081/SS-120027998**.

29 W. Nie, T. Wang, X. Gao, R. K. Pathak, X. Wang, R. Gao, Q. Zhang, L. Yang and W. Wang, Comparison among filter-based, impactor-based and continuous techniques for measuring atmospheric fine sulfate and nitrate, *Atmos. Environ.*, 2010, **44**, 4396–4403, DOI: **10.1016/j.atmosenv.2010.07.047**.

30 Environmental Protection Agency (EPA), **http://www.epa.gov/aqs**, accessed on 1 April 2022.

31 S. Oh, S.-G. Kim, J. B. Lee, J. Park, J.-B. Jee, S.-W. Hong, K.-S. Kwon and M. Song, Spatial distributions of atmospheric ammonia in a rural area in south Korea and the associated impact on a nearby urban area, *Atmosphere*, 2021, **12**, 1411, DOI: **10.3390/atmos12111411**.

32 ECOTECH, *Environmental monitoring, Serinus 40 oxides of Nitrogen analyzer, user manual, version 3.5*, **https://www.ecotech.com/**, accessed on 1 April 2022.

33 Korea Meteorological Administration (KMA), **https://data.kma.go.kr/cmmn/main.do**, accessed on 1 April 2022.

34 ISORROPIA, *version 2.1*, **http://nenes.eas.gatech.edu/ISORROPIA**, accessed on 1 April 2022.

35 C. Fountoukis and A. Nenes, ISORROPIA II: a computationally efficient thermodynamic equilibrium model for K^+–Ca^{2+}–Mg^{2+}–NH_4^+–Na^+–SO_4^{2-}–NO_3^-–Cl^-–H_2O aerosols, *Atmos. Chem. Phys.*, 2007, **7**, 4639–4659, DOI: **10.5194/acp-7-4639-2007**.

36 X. Jin, Y. Wang, Z. Li, F. Zhang, W. Xu, Y. Sun, X. Fan, G. Chen, H. Wu and J. Ren, Significant contribution of organics to aerosol liquid water content in winter in Beijing, China, *Atmos. Chem. Phys.*, 2020, **20**, 901–914, DOI: **10.5194/acp-20-901-2020**.

37 Y. B. Lim, J. Seo, J. Y. Kim, Y. P. Kim and H. C. Jin, Local formation of sulfates contributes to the urban haze with regional transport origin, *Environ. Res. Lett.*, 2020, **15**, 084034, DOI: **10.1088/1748-9326/ab83aa**.

38 W. Li, X. Teng, X. Chen, L. Liu, L. Xu, J. Zhang, Y. Wang, Y. Zhang and Z. Shi, Organic coating reduces hygroscopic growth of phase-separated aerosol particles, *Environ. Sci. Technol.*, 2021, **55**, 16339–16346, DOI: **10.1021/acs.est.1c05901**.

39 J. Sun, L. Liu, L. Xu, Y. Wang, Z. Wu, M. Hu, Z. Shi, Y. Li, X. Zhang and J. Chen, Key role of nitrate in phase transitions of urban particles: implications of important reactive surfaces for secondary aerosol formation, *J. Geophys. Res.: Atmos.*, 2018, **123**, 1234–1243, DOI: **10.1002/2017JD027264**.

© 2023 The Author(s). Published by the Royal Society of Chemistry

Environ. Sci.: Atmos., 2023, **3**, 422–433 | 431

40 J. Seo, Y. B. Lim, D. Youn, J. Y. Kim and H. C. Jin, Synergistic enhancement of urban haze by nitrate uptake into transported hygroscopic particles in the Asian continental outflow, *Atmos. Chem. Phys.*, 2020, **20**, 7575–7594, DOI: **10.5194/acp-20-7575-2020**.

41 W. Xu, Q. Wu, X. Liu, A. Tang, A. J. Dore and M. R. Heal, Characteristics of ammonia, acid gases, and $PM_{2.5}$ for three typical land-use types in the North China Plain, *Environ. Sci. Pollut. Res.*, 2016, **23**, 1158–1172, DOI: **10.1007/s11356-015-5648-3**.

42 P. Acharja, K. Ali, D. K. Trivedi, P. Safai, S. Ghude, T. Prabhakaran and M. Rajeevan, Characterization of atmospheric trace gases and water soluble inorganic chemical ions of PM_1 and $PM_{2.5}$ at Indira Gandhi International Airport, New Delhi during 2017–18 winter, *Sci. Total Environ.*, 2020, **729**, 138800, DOI: **10.1016/j.scitotenv.2020.138800**.

43 Z. Meng, X. Xu, W. Lin, B. Ge, Y. Xie, B. Song, S. Jia, R. Zhang, W. Peng and Y. Wang, Role of ambient ammonia in particulate ammonium formation at a rural site in the North China Plain, *Atmos. Chem. Phys.*, 2018, **18**, 167–184, DOI: **10.5194/acp-18-167-2018**.

44 J. Bahino, V. Yoboué, C. Galy-Lacaux, M. Adon, A. Akpo, S. Keita, C. Liousse, E. Gardrat, C. Chiron and M. Ossohou, A pilot study of gaseous pollutants' measurement (NO_2, SO_2, NH_3, HNO_3 and O_3) in Abidjan, Côte d'Ivoire: contribution to an overview of gaseous pollution in African cities, *Atmos. Chem. Phys.*, 2018, **18**, 5173–5198, DOI: **10.5194/acp-18-5173-2018**.

45 Y. Li, F. M. Schwandner, H. J. Sewell, A. Zivkovich, M. Tigges, S. Raja, S. Holcomb, J. V. Molenar, L. Sherman and C. Archuleta, Observations of ammonia, nitric acid, and fine particles in a rural gas production region, *Atmos. Environ.*, 2014, **83**, 80–89, DOI: **10.1016/j.atmosenv.2013.10.007**.

46 M. Mozurkewich, The dissociation constant of ammonium nitrate and its dependence on temperature, relative humidity and particle size, *Atmos. Environ., Part A*, 1993, **27**, 261–270, DOI: **10.1016/0960-1686(93)90356-4**.

47 J. Neuman, J. Nowak, C. Brock, M. Trainer, F. Fehsenfeld, J. Holloway, G. Hübler, P. Hudson, D. Murphy and D. Nicks Jr, Variability in ammonium nitrate formation and nitric acid depletion with altitude and location over California, *J. Geophys. Res.: Atmos.*, 2003, **108**, 4557, DOI: **10.1029/2003JD003616**.

48 Y. Chang, Z. Zou, Y. Zhang, C. Deng, J. Hu, Z. Shi, A. J. Dore and J. L. Collett Jr, Assessing contributions of agricultural and nonagricultural emissions to atmospheric ammonia in a Chinese megacity, *Environ. Sci. Technol.*, 2019, **53**, 1822–1833, DOI: **10.1021/acs.est.8b05984**.

49 C. Loftus, M. Yost, P. Sampson, E. Torres, G. Arias, V. B. Vasquez, K. Hartin, J. Armstrong, M. Tchong-French and S. Vedal, Ambient ammonia exposures in an agricultural community and pediatric asthma morbidity, *Epidemiology*, 2015, **26**, 794, DOI: **10.1097/EDE.0000000000000368**.

50 Y. Sun, Q. Jiang, Z. Wang, P. Fu, J. Li, T. Yang and Y. Yin, Investigation of the sources and evolution processes of severe haze pollution in Beijing in January 2013, *J. Geophys. Res.: Atmos.*, 2014, **119**, 4380–4398, DOI: **10.1002/2014JD021641**.

51 H. Zhang, S. Cheng, X. Wang, S. Yao and F. Zhu, Continuous monitoring, compositions analysis and the implication of regional transport for submicron and fine aerosols in Beijing, China, *Atmos. Environ.*, 2018, **195**, 30–45, DOI: **10.1016/j.atmosenv.2018.09.043**.

52 G. Zheng, H. Su, S. Wang, M. O. Andreae, U. Pöschl and Y. Cheng, Multiphase buffer theory explains contrasts in atmospheric aerosol acidity, *Science*, 2020, **369**, 1374–1377, DOI: **10.1126/science.aba3719**.

53 M. Tian, H. Wang, Y. Chen, F. Yang, X. Zhang, Q. Zou, R. Zhang, Y. Ma and K. He, Characteristics of aerosol pollution during heavy haze events in Suzhou, China, *Atmos. Chem. Phys.*, 2016, **16**, 7357–7371, DOI: **10.5194/acp-16-7357-2016**.

54 C. Fountoukis, A. Nenes, A. Sullivan, R. Weber, T. V. Reken, M. Fischer, E. Matías, M. Moya, D. Farmer and R. Cohen, Thermodynamic characterization of Mexico City aerosol during MILAGRO 2006, *Atmos. Chem. Phys.*, 2009, **9**, 2141–2156, DOI: **10.5194/acp-9-2141-2009**.

55 Z. Xu, M. Liu, M. Zhang, Y. Song, S. Wang, L. Zhang, T. Xu, T. Wang, C. Yan and T. Zhou, High efficiency of livestock ammonia emission controls in alleviating particulate nitrate during a severe winter haze episode in northern China, *Atmos. Chem. Phys.*, 2019, **19**, 5605–5613, DOI: **10.5194/acp-19-5605-2019**.

56 A. H. Souri, Y. Choi, W. Jeon, J. H. Woo, Q. Zhang and J. i. Kurokawa, Remote sensing evidence of decadal changes in major tropospheric ozone precursors over East Asia, *J. Geophys. Res.: Atmos.*, 2017, **122**, 2474–2492, DOI: **10.1002/2016JD025663**.

57 C. Hendriks, R. Kranenburg, J. Kuenen, B. Van den Bril, V. Verguts and M. Schaap, Ammonia emission time profiles based on manure transport data improve ammonia modelling across north western Europe, *Atmos. Environ.*, 2016, **131**, 83–96, DOI: **10.1016/j.atmosenv.2016.01.043**.

58 C. Bae, B.-U. Kim, H. C. Kim, C. Yoo and S. Kim, Long-range transport influence on key chemical components of $PM_{2.5}$ in the Seoul metropolitan area, South Korea, during the years 2012–2016, *Atmosphere*, 2019, **11**, 48, DOI: **10.3390/atmos11010048**.

59 S. Lv, F. Wang, C. Wu, Y. Chen, S. Liu, S. Zhang, D. Li, W. Du, F. Zhang and H. Wang, Gas-to-Aerosol Phase Partitioning of Atmospheric Water-Soluble Organic Compounds at a Rural Site in China: An Enhancing Effect of NH_3 on SOA Formation, *Environ. Sci. Technol.*, 2022, **56**, 3915–3924, DOI: **10.1021/acs.est.1c06855**.

60 M. Li, Z. Zhang, Q. Yao, T. Wang, M. Xie, S. Li, B. Zhuang and Y. Han, Nonlinear responses of particulate nitrate to NO_x emission controls in the megalopolises of China, *Atmos. Chem. Phys.*, 2021, **21**, 15135–15152, DOI: **10.5194/acp-21-15135-2021**.

61 X. Fu, T. Wang, J. Gao, P. Wang, Y. Liu, S. Wang, B. Zhao and L. Xue, Persistent heavy winter nitrate pollution driven by increased photochemical oxidants in northern China, *Environ. Sci. Technol.*, 2020, **54**, 3881–3889, DOI: **10.1021/acs.est.9b07248**.

62 C. Womack, E. McDuffie, P. Edwards, R. Bares, J. de Gouw, K. Docherty, W. Dubé, D. Fibiger, A. Franchin and J. Gilman, An odd oxygen framework for wintertime ammonium nitrate aerosol pollution in urban areas: NO_x and VOC control as mitigation strategies, *Geophys. Res. Lett.*, 2019, **46**, 4971–4979, DOI: **10.1029/2019GL082028**.

© 2023 The Author(s). Published by the Royal Society of Chemistry

Environ. Sci.: Atmos., 2023, **3**, 422–433 | **433**